Mutually tangled colloidal knots and induced defect loops in nematic fields

Angel Martinez[1,2], Miha Ravnik[3], Brice Lucero[1], Rayshan Visvanathan[1], Slobodan Žumer[3,4] and Ivan I. Smalyukh[1,2,5,6]★

Colloidal dispersions in liquid crystals can serve as a soft-matter toolkit for the self-assembly of composite materials with pre-engineered properties and structures that are highly dependent on particle-induced topological defects[1-3]. Here, we demonstrate that bulk and surface defects in nematic fluids can be patterned by tuning the topology of colloidal particles dispersed in them. In particular, by taking advantage of two-photon photopolymerization techniques to make knot-shaped microparticles, we show that the interplay of the topologies of the knotted particles, the nematic field and the induced defects leads to knotted, linked and other topologically non-trivial field configurations[4-12]. These structures match theoretical predictions made on the basis of the minimization of the elastic free energy and satisfy topological constraints[4,5]. Our approach may find uses in self-assembled topological superstructures of knotted particles linked by nematic fields, in topological scaffolds supporting the decoration of defect networks with nanoparticles[1], and in modelling other physical systems exhibiting topologically analogous phenomena[12-16].

One of the grand challenges of modern material science is to design and assemble three-dimensional (3D) structures of low-symmetry colloidal particles that can reproduce complex behaviour of atomic systems with different types of bonding and a large number of chemical elements[15-24]. Interestingly, long before the nature of atoms could be understood, early mathematical developments of knot theory, one of the key branches of topology, were prompted by Lord Kelvin's conjecture from 1867 that atoms of all elements were different knotted defect lines known as 'vortices'[4,5,12]. Although our modern understanding of atoms is very different and naturally occurring materials are not just tangled knots of defects, applications of the mathematical knot theory are nowadays found in many branches of science, including material systems such as liquid crystals, cosmology, quantum chromodynamics, and both classical and quantum field theories[3-11]. However, there are few theoretical predictions involving knotted fields and vortices that can be tested by experiments[9], which is due to the lack of systems and techniques that allow for controlling types and spatial arrangements of defects in three dimensions. On the other hand, mastering control of topological defects in liquid crystals is also important from a practical standpoint because they are key for mediating nanoscale confinement and mesoscale self-assembly of nanoparticles[1,17-23].

In this work, we develop knotted nematic colloids that enable the generation and control of 3D patterns of point defects and configurations of looped line defects, such as tangled knots, thus allowing for experimental insights into predictions from knot theory and into the interplay of topologies of knotted surfaces, fields and defects[4,5]. On the one hand, this may be used for understanding other experimentally less accessible physical systems with similar topology, ranging from particle physics to cosmology[13-16]. On the other hand, our knotted colloids can be used as building blocks of topological matter, this arising from the mesoscale self-organization of knotted colloidal 'atoms' driven by the minimization of elastic free energy and from the mutual entanglement of induced defects. Particle-controlled configurations of defects may also serve as topologically non-trivial scaffolds for the 3D patterning of semiconductor and metal nanoparticles[1], as needed for the scalable fabrication of composite materials with pre-designed properties. Our findings show that the behaviour of knotted colloidal 'atoms' obeys topological constraints, and, therefore, that topological theorems and mathematical knot theory can be used to guide the design of self-assembled knotted matter as envisaged by Kelvin[12].

Colloids are stable dispersions of microscopic particles in host media[16], which in the case of nematic colloids consist of particles dispersed in a host fluid of anisotropic liquid-crystal molecules that spontaneously align along the director $\mathbf{n}$ (refs 17–23). Colloidal particles can also be anisotropic, typically in terms of the shape and chemical functionalization of their surfaces. Anisotropic particles were central to recent efforts of reproducing the complexity of atomic bonding in self-assembled colloidal structures[24] and of generating biomimetic self-propulsion capabilities[25]. However, all anisotropic colloids made so far exhibit relatively high symmetry, and colloidal synthesis typically offers limited control of surface topology[23]. Here, we use two-photon photopolymerization with spatially patterned pulsed femtosecond laser light (see Methods and Supplementary Fig. 1)[26] to obtain rigid particles with the surface topology of torus knots $T(p,q)$. The particles are formed by knotted polymeric tubes that, before having their ends joined, are looped p times through the hole of an imaginary torus, with q revolutions about the torus rotational symmetry axis[4,5] (Fig. 1). The minimum number of crossings of the polymeric tube in these particles is given by the so-called crossing number $c = \min\{p(q-1), q(p-1)\}$. When dispersed in liquid crystals, these knotted colloids with controlled surface boundary conditions distort the director field $\mathbf{n}(\mathbf{r})$, which

[1]Department of Physics, University of Colorado, Boulder, Colorado 80309, USA, [2]Liquid Crystal Materials Research Center, University of Colorado, Boulder, Colorado 80309, USA, [3]Faculty of Mathematics and Physics, University of Ljubljana, Jadranska 19, Ljubljana 1000, Slovenia, [4]Jozef Stefan Institute, Jamova 39, Ljubljana 1000, Slovenia, [5]Department of Electrical, Computer, and Energy Engineering and Materials Science and Program, University of Colorado, Boulder, Colorado 80309, USA, [6]Renewable and Sustainable Energy Institute, National Renewable Energy Laboratory and University of Colorado, Boulder, Colorado 80309, USA. *e-mail: ivan.smalyukh@colorado.edu
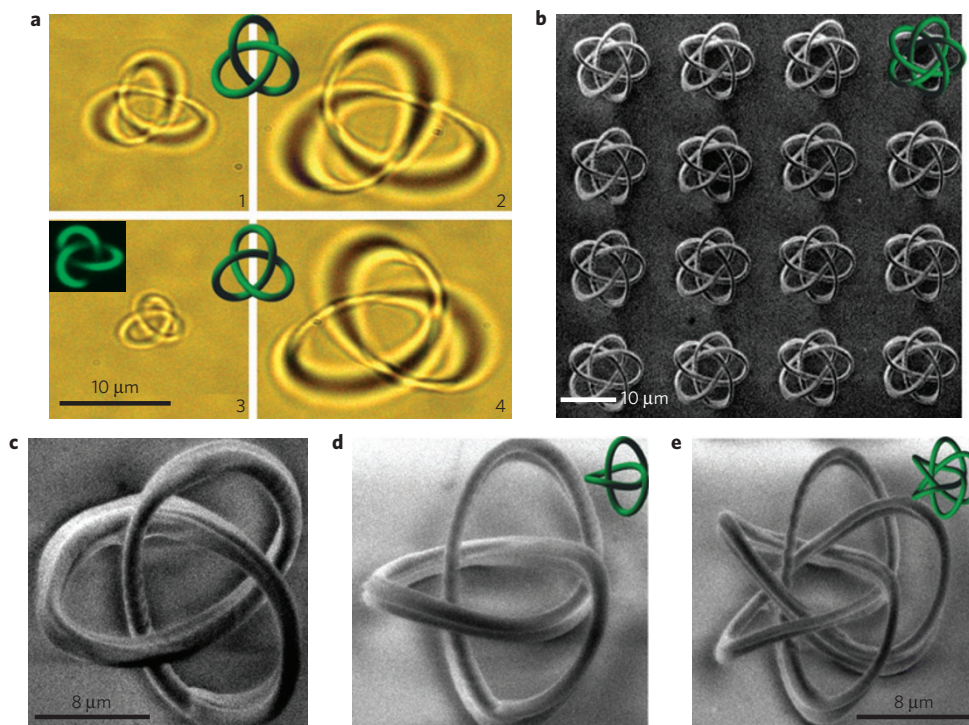
Figure 1 | Photopolymerized knotted particles and their arrays. a, Optical micrographs showing photopolymerized left-handed (panels 1 and 2) and right-handed (panels 3 and 4) trefoil colloidal torus knots $T(3,2)$ with $c = 3$ and of different sizes, with the corresponding 3D models shown in green. The top-left inset in panel 3 shows a 3PEF-PM image of a colloidal particle of the same chirality and comparable size as that shown on the same panel. Micrographs show particles being slightly larger than their actual size because of the limited optical resolution. **b**, Scanning electron micrograph of a 4×4 array of torus knots $T(5,3)$ with $c = 10$ on a glass substrate. **c–e**, Zoomed-in scanning electron micrographs of single $T(3,2)$ (**c,d**) and $T(5,3)$ (**e**) knots shown from different perspectives, along with the corresponding 3D models (depicted in green), as viewed along the torus axis (**c**) and in an oblique direction (**d,e**).

approaches the uniform far-field director $\mathbf{n}_0$ at large distances. 3D visualization of $\mathbf{n}(\mathbf{r})$ by means of nonlinear optical polarizing microscopy (Supplementary Figs 2 and 3), assisted by holographic optical tweezers[27,28], reveals a topological interplay among surfaces of knotted particles, nematic fields and defects.

Nematic dispersions of trefoil particle knots—known more formally as $T(3,2)$ torus knots and also as 3_1 knots in the Alexander–Briggs notation[4]—are first explored in the regime where the nematic molecular orientation field at the particle surfaces is set to be tangential. In a stable configuration, which corresponds to the minimum of free energy, the trefoil colloids align with their torus plane perpendicular to the undistorted far-field nematic director $\mathbf{n}_0$. As their complex shape is incompatible with the inherently homogeneous field of the aligned nematic liquid crystal, point defects called 'boojums' emerge at the surfaces of the particles, and are visible in bright-field micrographs as dark points due to scattering (Fig. 2a). Polarizing microscopy textures show smooth variations of the molecular orientation field everywhere in the sample, except at the boojums (Fig. 2b,c). Using the three-photon excitation fluorescence polarizing microscopy (3PEF-PM) technique with polarized laser excitation[27,28], we explore the full 3D molecular orientation field (Fig. 2d,g) by probing high-intensity fluorescence patterns (originating from both the polymer in the particle and the surrounding liquid crystal with director distortions) shaped as trefoil knots with elliptical cross-sections, which reveal the strongest director distortions in regions where colloidal surfaces are orthogonal to $\mathbf{n}_0$, consistent with numerical modelling (Fig. 2g–i and Supplementary Fig. 4). Experimental 3PEF-PM textures in individual cross-sectional planes closely match their simulated counterparts, as shown for a sample region near boojums in Fig. 2d–g. To clearly identify positions of the surface defects, a

colour-coded 3D representation of the azimuthal orientation of the director field around the particle is constructed, which reveals 12 boojums, forming nearby regions where the particle's surface is orthogonal to the far-field director (Fig. 2h). These boojums can be characterized by a winding number s of the 2D director field at the liquid-crystal/particle interface and also by the bulk topological charge m (refs 16,23,29). The winding number is an invariant commonly used to characterize 2D profiles of a field surrounding a defect—in our case, the field profile at the surface of the particle knot—and defines the number of times the director rotates by 2π as one circumnavigates the defect core once. The nonpolar symmetry of the nematic director field allows integer numbers of π turns of the director around the defects, with positive and negative signs identifying defects with the director rotation being the same as or opposite to that of circumnavigation, respectively. The topological charge m is used to characterize point defects and loops of defect lines in three dimensions, and is a characteristic similar to s but describing the variation in the director-field profile around the defect objects in all three spatial dimensions. Its magnitude can be calculated using a simple integral of the director structure over an enclosing surface[16,23]. By experimentally mapping and calculating the molecular orientational profile in the bulk and at surfaces around these defects, in agreement with topological theorems[4,23], we find $\Sigma_i s_i = \chi = 0$, where i runs over all boojums and $\chi = 0$ is the Euler characteristic of the knotted particle surface. Although this topological constraint could be satisfied in many different ways, the one observed experimentally corresponds to a local or global minimum of the total free energy. Both experiments and numerical modelling reveal that the stable field configuration around a trefoil particle knot with tangential boundary conditions contains 12 surface point defects: six $s = 1$
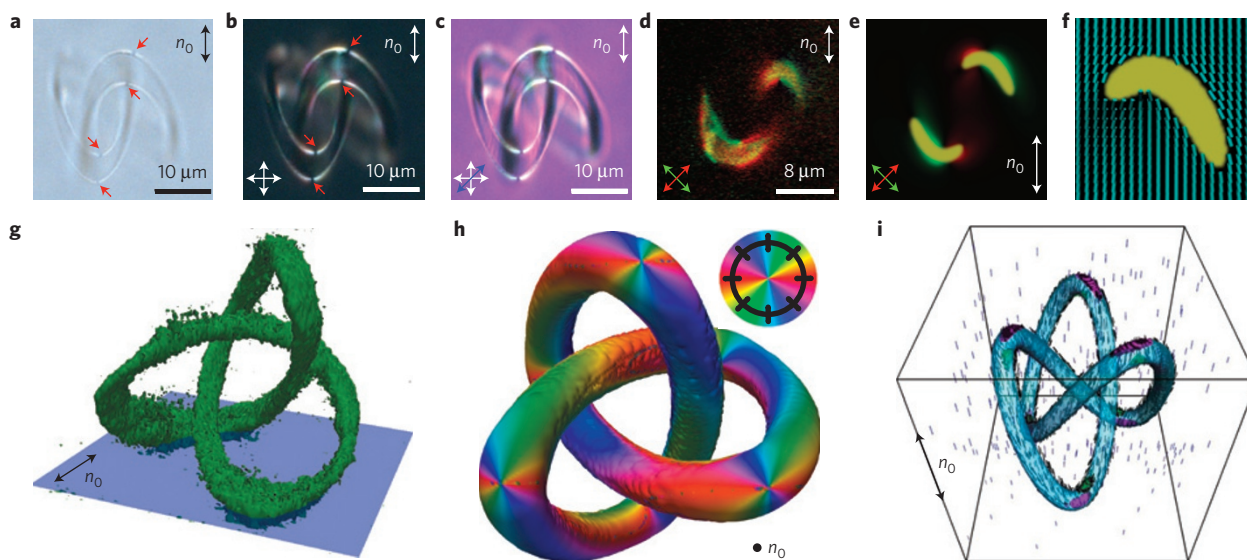
Figure 2 | A trefoil knot particle with tangential boundary conditions in an aligned liquid crystal. a–c, Bright-field and polarizing optical micrographs taken without polarizers (**a**), between crossed polarizers whose directions are shown by white double arrows (**b,c**), and with an additional 530 nm retardation plate having its slow axis aligned as shown by the blue double arrow (**c**). Locations of boojums are marked by red arrows in **a,b**. **d,e,** 3PEF-PM slices obtained experimentally (**d**) and by numerical modelling (**e**). Each colour within these superimposed images (green and red) represents the fluorescence signal from a single 3PEF-PM scan with imaging beam polarizations aligned along the colour-coded directions shown by double arrows. **f,** Computer-simulated $\mathbf{n}(\mathbf{r})$ within the top-right part of the cross-section shown in (**d,e**). **g,** 3D fluorescence pattern of the knotted particle and surrounding director distortions reconstructed from 3PEF-PM scans. The blue plane indicates the location of the single-slice images shown in **d,e**. **h,** 3D representation of $\mathbf{n}(\mathbf{r})$ deviating away from $\mathbf{n_0}$ due to the incorporated trefoil knot particle. Colours depict the azimuthal orientation of $\mathbf{n}(\mathbf{r})$ when projected onto a plane orthogonal to $\mathbf{n_0}$ and according to the scheme shown in the inset. The structure is visualized on a tube following the knotted particle's surface. Points where different colours meet are boojums. **i,** 3D representation of computer-simulated $\mathbf{n}(\mathbf{r})$ at the particle/liquid-crystal interface (black rods) and in the bulk (blue rods) induced by a trefoil knot particle. Green and magenta areas show regions of a reduced scalar order parameter of 0.42, corresponding to $s = -1$ and $s = 1$ 2D defects at the liquid-crystal/particle interface, respectively. The knots in **g–i** are shown from different perspectives in order to depict different features of the ordering.

boojums, which localize on the exterior tips of the knot, and their six $s = -1$ counterparts, which reside on the diametrically opposite sides of the knotted tube (the corresponding regions of the reduced scalar order parameter are depicted in Fig. 2i in magenta and green colours, respectively).

Trefoil particle knots with perpendicular surface boundary conditions align with a torus plane either orthogonal to $\mathbf{n_0}$ in the ground state or at several metastable orientations, including those parallel to $\mathbf{n_0}$ (Fig. 3 and Supplementary Fig. 5). These ground-state and metastable configurations, which correspond to global and local free-energy minima, respectively, can be accessed with the same particle by sequentially heating the sample with an objective-based temperature control system FCS-2 (from Bioptechs) to about 34 °C—which is right below the nematic–isotropic transition of the used liquid crystal—and then locally 'melting' the liquid crystal with a holographic optical-tweezers beam, followed by quenching it back to the nematic state. Optical micrographs of such a knotted particle are consistent with $\mathbf{n}(\mathbf{r})$ near its surface being normal to it (Fig. 3). 3PEF-PM imaging with excitation light polarized perpendicular to $\mathbf{n_0}$ yields a knotted tube of high intensity with an anisotropic cross-section (Supplementary Fig. 6). Individual depth-resolved 3PEF-PM 'slices' obtained for different polarizations show the presence of defect lines (marked by red arrows in Fig. 3d,e), which match our theoretical configuration with two singular $s = -1/2$ defect lines following the knotted tube (Fig. 3c,f). These defect lines compensate for the director imposed by the particle's surface, which resembles that of a knotted radial defect line with $s = 1$. Two linear defects tracing the knotted particle's tube is also the basic feature of all metastable states, although they are often accompanied by their rewirings and linking to the knotted particle (Fig. 3g–j and Supplementary Fig. 5). This shows that knotted particles can

generate defect loops in nematic fields by elastically distorting the liquid crystal in such a way that these loops are knotted too. For the $T(3, 2)$ particle shown in Fig. 3, the two defect loops are both $T(3, 2)$ torus knots, mutually linked into a two-component link. This link of line defects is further linked with the particle knot (inset of Fig. 3f), effectively forming a three-component defect–particle link. In mathematics, linking of two closed curves in 3D space is commonly described by an integer called the 'linking number'. Intuitively, this represents the number of times that each curve winds around the other, and it can be positive or negative, depending on the orientation of the two curves[5]. In a similar way, the observed linking of particles and defects can be characterized by two topological invariants: the linking number Ln of the particle with the induced defect loops in the nematic field, and the self-linking number Sl of the defect line, which labels how many times it turns around its tangent in the course of one loop[29]. The linking number of the particle knot with a chosen knotted defect loop $Ln = 3$ emerges to be equivalent to the self-linking number $Sl = 3$ of this loop, $Ln = Sl$, yielding a relation that connects the topology of the particle with that of the surrounding molecular field. This equivalence of two distinct topological invariants stems from the local compensation of the induced distortion—that is, the diametrically opposite elastic pinning of the two defect loops near the particle surface—and is valid for all studied particle knots with perpendicular boundary conditions, such as the $T(5, 2)$ and $T(7, 2)$ shown in Supplementary Fig. 7 (ref. 27), provided that the defects smoothly follow the particle's knotted tube without irregular rewirings (Supplementary Fig. 8). Interestingly, the linking number of the knotted particle with the surrounding defect loops can be controllably changed, for example by reorienting the knotted particle into one of the metastable states (Supplementary Fig. 5).
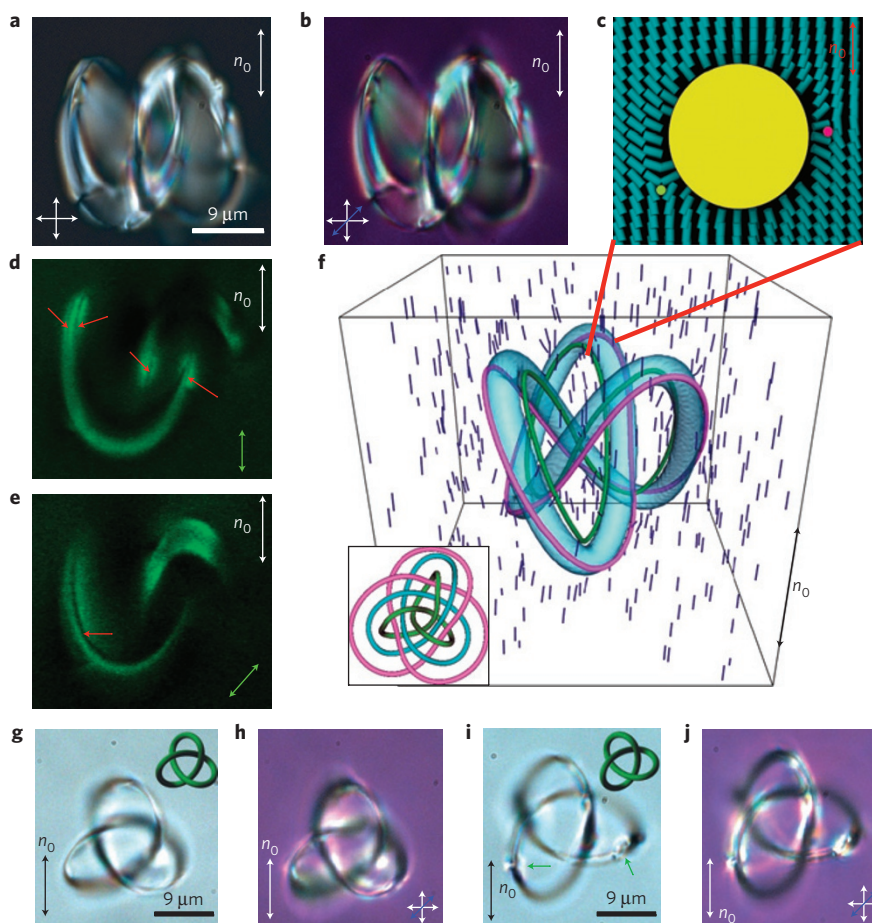
Figure 3 | A colloidal trefoil knot with perpendicular surface boundary conditions. a,b, Bright-field micrographs of a particle in an aligned nematic taken between crossed polarizers whose directions are indicated by the white arrows (**a,b**) and with a full-wave 530 nm retardation plate inserted with its slow axis at 45° (blue double arrow; **b**). **c,** Computer-simulated **n(r)** within a cross-section perpendicular to the knotted tube marked in **f. d,e,** 3PEF-PM images of **n(r)** around the knotted particle shown in **a,b** and for excitation-light polarizations (green double arrows) at different orientations with respect to **n₀**. Red arrows mark the defect lines. **f,** Computer-simulated **n(r)** around a trefoil knot with perpendicular boundary conditions and the torus plane orthogonal to **n₀**. Green and magenta lines show regions with reduced scalar order parameter corresponding to the cores of the two knotted defect lines seen in the cross-sections (**d,e**). The inset shows a topological schematic of the mutual linking between the particle knot (blue) and defect knots (green and magenta). **g–j,** Bright-field micrographs of colloidal knots aligned with the torus plane parallel to **n₀**, and taken without polarizers (**g,i**) and between crossed polarizers with an inserted full-wave retardation plate (**h,j**). Green arrows in **i** indicate the locations of the rewirings of defect lines, similar to the ones visible in the model shown in Supplementary Fig. 5u,v.

Another approach to characterize topological defect loops is by their topological charge[23,29]: the homogeneous far-field director sets the net total topological charge of the particle and the defect loops equal to zero, and the trefoil knot particle has Euler characteristic $\chi = 0$ (ref. 5), which also conditions the topological charge of the particle to be zero and puts the net topological charge of the two knotted defect loops equal to zero (under modulo 2; ref. 29). Indeed, these topological charges are also reproduced using a general formalism introduced in previous theoretical works[29].

Our study can be extended to colloidal knots of higher complexity, such as the colloids in the form of $T(5, 3)$ torus knots (10_{124} in the Alexander–Briggs notation) with the crossing number $c = 10$ that we show in Fig. 4 and Supplementary Fig. 9. These knotted particles with tangential anchoring induce boojums that obey the same topological constraint $\Sigma_i s_i = 0$ as their trefoil counterparts, because $\chi = 0$ for both, but the total number of boojums is now 20: 10 boojums with the winding number $s = 1$ and 10 with $s = -1$ defects in the 2D field at the liquid-crystal/particle interface. The $T(5, 2)$ torus knot particles also induce a total of 20 self-compensating boojums (Fig. 5). In general, the equilibrium **n(r)**-structures induced by torus knots with tangential anchoring

host $|4p|$ self-compensating defects. This behaviour for torus knots with $p = 3, 5, 7$ and larger persists when the knotted tube's diameter and overall particle dimensions are changed (Fig. 5 and Supplementary Fig. 10–12). However, in addition to the stable configurations, one also observes metastable states having different numbers and locations of boojums, yielding oblique orientations of the particle's torus plane relative to **n₀**, as we demonstrate using examples of several different knots shown in Supplementary Figs 13 and 14. Likewise, although the knotted particles with perpendicular boundary conditions and $p = 3, 5, 7$ and higher are typically accompanied by two knotted defect lines with $s = -1/2$, by changing the diameter of the knotted tube relative to the overall particle size one can also achieve metastable configurations in which the two defects exhibit different rewirings (Supplementary Fig. 8). This demonstrates that the topological constraints allow for flexibility in terms of the precise ways of satisfying them. Therefore, by varying confinement, using liquid-crystal materials with different elastic constants, temperature quenching and the application of external fields, one can create an experimental arena for exploiting the means of control of this behaviour. Finally, for all studied particles, field configurations and self-aligned
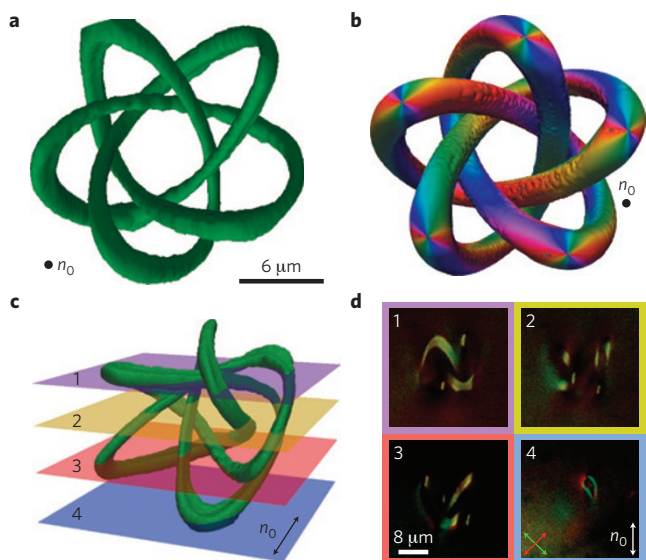
Figure 4 | A colloidal knot $T(5,3)$ with tangential boundary conditions.
a, 3D reconstruction of 3PEF-PM intensity for the $T(5,3)$ particle with director distortions around it. **b**, 3D representation of $\mathbf{n(r)}$ deviation from $\mathbf{n_0}$ around the particle. Colours depict the azimuthal orientation of $\mathbf{n(r)}$ projected onto a plane orthogonal to $\mathbf{n_0}$ according to the scheme shown in the inset of Fig. 2h. The structure is visualized on a tube following the surface of the colloidal knot. The points where different colours meet are boojums. **c**, A 3D perspective view of the $T(5,3)$ particle shown in **a**, with the four corresponding cross-sectional planes depicted in **d**. **d**, 3PEF-PM scans with superimposed green and red colour-coded fluorescence images obtained for linear polarizations of excitation light along the double arrows of the same colour marked in panel 4.

colloidal orientation states, the chiral nature of knotted colloids causes mirror-symmetry breaking in the induced director field $\mathbf{n(r)}$, potentially allowing for the self-assembly of chiral colloidal superstructures in non-chiral nematic liquid crystals.

Knots have been realized in the past either as material objects, such as knots of small molecules and polymer strands, or as knotted fields, whereas our nematic colloids can be a combination of both because the nematic field is guided by the particle knot. For perpendicular boundary conditions, the particle knot is even physically linked with the defect knots of the field, having particle-to-defect-loop linking number $Ln = 3$. Importantly, knotted particles energetically stabilize complex (knotted) nematic fields in time and space, allowing one to probe the details of their structure, which cannot be achieved in other knotted fields[7]. For example, as already envisaged by Kelvin, vortex lines in a fluid flow remain stable in time only if the fluid is 'perfectly destitute of viscosity'[12]; in real fluids this always fails and knots decay in time[7]. In particle physics, glueballs are theoretically modelled as knotted flux tubes[30], but even the very experimental verification of glueball existence, not to mention probing their internal structure, is extremely difficult despite the advances in modern particle accelerators. Therefore, our colloidal knots offer the exciting opportunity of providing experimental insights into the physical realization of predictions from knot theory and its links to physical and material systems.

To conclude, we realized a colloidal system of particle knots coupled to nematic fields, providing insights into the interplay of their topologies. This interplay is controlled by varying surface boundary conditions and prompts the formation of topological defects, including boojums and knots of defect lines. The particles and field structures—for example, defect lines—can get mutually tangled, forming linked particle–field knots. Large quantities
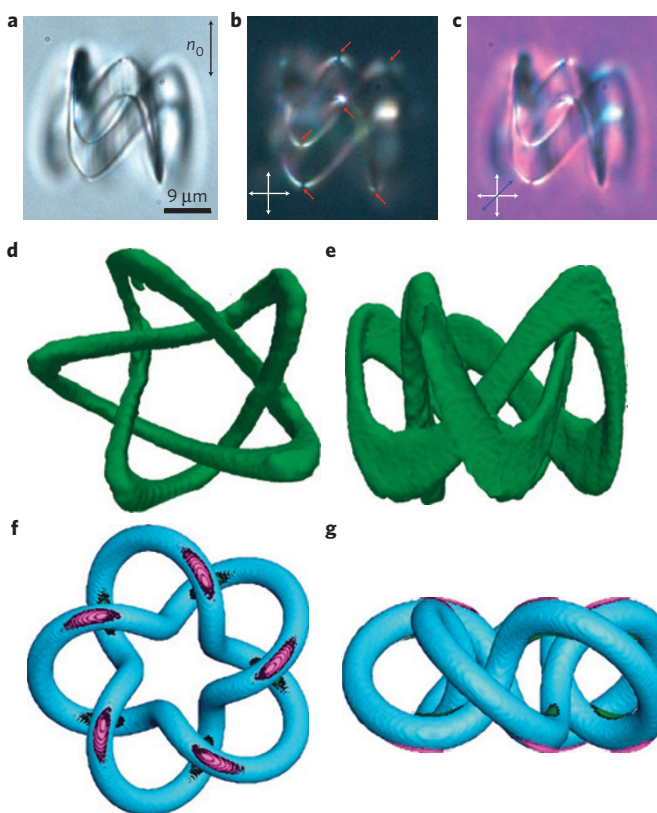

Figure 5 | Torus knot $T(5,2)$ particles with tangential boundary conditions. a–c, Optical micrographs of the $T(5,2)$ knotted particle obtained without polarizers (**a**), with crossed polarizers aligned as indicated by the white double arrows (**b**), and with crossed polarizers and an additional phase retardation plate (blue double arrow) aligned with its slow axis at 45° to crossed polarizers and $\mathbf{n_0}$ (**c**). Locations of boojums visible within the optical micrographs are marked by red arrows in **b**. **d,e**, Two different perspective views of the reconstructed 3PEF-PM intensity pattern due to the $T(5,2)$ colloidal knot particle and director distortions induced by the particle as viewed along the torus axis (**d**) and perpendicular to it (**e**). **f,g**, Numerical model showing surface defects induced by a $T(5,2)$ particle as viewed along the torus axis (**f**) and in a direction perpendicular to it (**g**). Green and magenta areas show regions of a reduced scalar order parameter of 0.42, corresponding to $s = -1$ and $s = 1$ defects in the 2D director field at the liquid-crystal/particle interface, respectively.

of colloidal knots can be obtained by combining two-photon photopolymerization with structured shaping of femtosecond laser light via spatial light modulators[28]. Therefore, our knotted colloids represent a vision towards the incomparable topological matter made of self-assembled knots envisaged by Kelvin[12]. As the types of particle-induced defect are governed by the topology of knotted particles, these relations can be exploited to generate 3D patterns of vortices with varied symmetry and complexity, both at the surfaces of these particles and in the liquid-crystal bulk around them. On the one hand, these defects can mediate colloidal self-assembly by means of both anisotropic elastic forces[17–23] and entanglement[29]. On the other hand, particle-induced defects can mediate the generation of free-energy landscapes for nanoparticle entrapment[1], thus allowing one to controllably decorate the colloidal knots with metal and semiconductor nanoparticles, which may provide a means for achieving the hierarchical self-assembly of new topological composite materials. Therefore, by establishing general principles for the 3D control of defects, the demonstrated interplay of topologies of knotted colloidal

surfaces and nematic fields provides a basis for highly unusual yet practically useful forms of self-assembly, potentially impinging on the design of mesoscale composite materials and applications, ranging from a new breed of information displays to metamaterials, nanophotonics and data storage.

Methods

Sample preparation. Colloidal particles in the form of thin, rigid polymeric tubes shaped into knots of different chiralities (Fig. 1) were fabricated at rates of about 1,000 particles per hour using the automated set-up shown in Supplementary Fig. 1, as described in detail in the Supplementary Information[26]. Each $T(p,q)$ torus knot particle was obtained by looping p times a focused photopolymerizing laser beam through the hole of an imaginary torus, with q revolutions about the torus before joining the ends of the ensuing polymerized knotted tube. The tube diameter was tuned from 0.3 to 3 μm and the overall size of particles was varied from 3 to 15 μm. The particles were dispersed in either a single-compound nematic liquid crystal pentylcyanobiphenyl (5CB) or in a mixture ZLI-2806 (both from EM Chemicals). As-manufactured colloidal knots induced strong tangential surface boundary conditions, but some of them were chemically treated to induce perpendicular ones[26]. Colloidal dispersions were confined into 25–50 μm cells made of parallel glass plates with inner surfaces treated to induce strong planar or perpendicular boundary conditions for **n(r)**. Nematic fields around knotted particles were studied using the 3PEF-PM set-up shown in Supplementary Fig. 2 (refs 27,28). 3PEF-PM images shown in Figs 2–5 and Supplementary Movies 1–3 generated from such 3PEF-PM images depict fluorescence signals arising due to the nonlinear optical excitation of the dispersion. Unlike the (isotropic) IP-L polymer inside particles, nematic host 5CB (Supplementary Fig. 3a) exhibits a strong well-defined dependence of the fluorescence intensity on the orientation of the linear polarization of the probe beam. Close analysis of polarization-dependent 3PEF-PM image stacks (Supplementary Movie 1) composed of individual optical 'slices', such as the ones presented in Figs 2d, 3d,e and 4d, reveals that the induced **n(r)** and defects depend on the boundary conditions and topology of the colloidal surfaces.

Numerical and topological modelling. The coupling between colloidal surfaces and **n(r)** is also explored by a numerical approach based on Landau–de Gennes free-energy minimization. This approach phenomenologically combines surface anchoring effects together with phase properties, nematic elasticity, variable degree of nematic order and its biaxiality into a free-energy functional based on the order parameter tensor Q_{ij} (refs 16,22). Being particularly effective at micrometre scales and when modelling complex shapes, it allows for the theoretical characterization of **n(r)** and defect-induced variations in nematic ordering that correspond to global or local minima of the free energy. Knotted particles are defined by an implicit declaration of knots and by assigning a fixed thickness to this definition. Minimization of the free energy is performed numerically for both tangential and perpendicular boundary conditions using an explicit finite-difference scheme on a cubic mesh[27]. This procedure yields spatial variations of the scalar order parameter and biaxiality in regions of defects and stable or metastable director fields **n(r)**. They are subsequently used to computer-simulate 3PEF-PM textures with experimental imaging resolution[27,28], allowing for a direct comparison of theory and experiments (Figs 2–5).

References

1. Senyuk, B. *et al.* Shape-dependent oriented trapping and scaffolding of plasmonic nanoparticles by topological defects for self-assembly of colloidal dimers in liquid crystals. *Nano Lett.* **12,** 955–963 (2012).
2. Alexander, G. P., Chen, B. G., Matsumoto, E. A. & Kamien, R. D. Colloquium: Disclination loops, point defects, and all that in nematic liquid crystals. *Rev. Mod. Phys.* **84,** 497–514 (2012).
3. Tkalec, U., Ravnik, M., Čopar, S., Žumer, S. & Muševič, I. Reconfigurable knots and links in chiral nematic colloids. *Science* **333,** 62–65 (2011).
4. Livingston, C. *Knot Theory* (The Mathematical Association of America, Indiana University-Bloomington, 1993).
5. Kauffman, L. H. *Knots and Physics* 3rd edn (World Scientific, 2000).
6. Dennis, M. R., King, R. P., Jack, B., O'Holleran, K. & Padgett, M. J. Isolated optical vortex knots. *Nature Phys.* **6,** 118–121 (2010).
7. Kleckner, D. M. & Irvine, W. T. Creation and dynamics of knotted vortices. *Nature Phys.* **9,** 253–258 (2013).
8. Yi-Shi, D., Li, Z. & Xin-Hui, Z. Topological structure of knotted vortex lines in liquid crystals. *Commun. Theor. Phys.* **47,** 1129–1134 (2007).
9. Faddeev, L. & Niemi, A. J. Stable knot-like structures in classical field theory. *Nature* **387,** 58–61 (1997).
10. Bouligand, Y., Derrida, B., Poenaru, V., Pomeau, Y. & Toulouse, G. Distortions with double topological character: The case of cholesterics. *J. Physique* **39,** 863–867 (1978).
11. Smalyukh, I. I., Lansac, Y., Clark, N. & Trivedi, R. Three-dimensional structure and multistable optical switching of triple twist Toron quasiparticles in anisotropic fluids. *Nature Mater* **9,** 139–145 (2010).
12. Thomson, W. On vortex atoms. *Phil. Mag.* **34,** 15–24 (1867).
13. Chuang, I., Durrer, R., Turok, N. & Yurke, B. Cosmology in the laboratory: Defect dynamics in liquid crystals. *Science* **251,** 1336–1342 (1991).
14. Bowick, M. J., Chandar, L., Schiff, E. A. & Srivastava, A. M. The cosmological Kibble mechanism in the laboratory: string formation in liquid crystals. *Science* **263,** 943–945 (1994).
15. Alsayed, A. M., Islam, M. F., Zhang, J., Collings, P. J. & Yodh, A. G. Premelting at defects within bulk colloidal crystals. *Science* **309,** 1207–1210 (2005).
16. Chaikin, P. M. & Lubensky, T. C. *Principles of Condensed Matter Physics* (Cambridge Univ. Press, 2000).
17. Poulin, P., Holger, S., Lubensky, T. C. & Weitz, D. A. Novel colloidal interactions in anisotropic fluids. *Science* **275,** 1770–1773 (1997).
18. Nelson, D. R. Toward a tetravalent chemistry of colloids. *Nano Lett.* **2,** 1125–1129 (2002).
19. Loudet, J. C., Barois, P. & Poulin, P. Colloidal ordering from phase separation in a liquid-crystalline continuous phase. *Nature* **407,** 611–613 (2000).
20. Martinez, A., Mireles, H. C. & Smalyukh, I. I. Large-area optoelastic manipulation of colloidal particles in liquid crystals using photoresponsive molecular surface monolayers. *Proc. Natl Acad. Sci. USA* **108,** 20891–20896 (2011).
21. Wood, T. A., Lintuvuori, J. S., Schofield, A. B., Marenduzzo, D. & Poon, W. C. K. A self-quenched defect glass in a colloid-nematic liquid crystal composite. *Science* **334,** 79–83 (2011).
22. Ravnik, M. & Žumer, S. Landau–de Gennes modelling of nematic liquid crystal colloids. *Liq. Cryst.* **36,** 1201–1214 (2009).
23. Senyuk, B. *et al.* Topological colloids. *Nature* **493,** 200–205 (2013).
24. Wang, Y. *et al.* Colloids with valence and specific directional bonding. *Nature* **491,** 51–55 (2012).
25. Marchetti, M. C. *et al.* Hydrodynamics of soft active matter. *Rev. Mod. Phys.* **85,** 1143–1189 (2013).
26. Martinez, A., Lee, T., Asavei, Th., Rubinsztein-Dunlop, H. & Smalyukh, I. I. Three-dimensional complex-shaped photopolymerized microparticles at liquid crystal interfaces. *Soft Matter* **8,** 2432–2437 (2012).
27. Lee, T., Trivedi, R. P. & Smalyukh, I. I. Multimodal nonlinear optical polarizing microscopy of long-range molecular order in liquid crystals. *Opt. Lett.* **35,** 3447–3449 (2010).
28. Trivedi, R. P., Lee, T., Bertness, K. & Smalyukh, I. I. Unconventional structure-assisted optical manipulation of high-index nanowires in liquid crystals. *Opt Express* **18,** 27658–27669 (2010).
29. Čopar, S. & Žumer, S. Nematic baids: Topological invariants and rewiring of disclinations. *Phys. Rev. Lett.* **106,** 177801 (2011).
30. Buniy, R. V. & Kephart, T. Glueballs and the universal energy spectrum of tight knots and links. *Int. J. Mod. Phys. A* **20,** 1252–1259 (2005).

Author contributions

A.M., B.L., R.V. and I.I.S. performed experimental work and analysed experimental results. A.M. built the two-photon polymerization set-up. M.R. and S.Ž. carried out numerical modelling of the structures of defects and fields. A.M. and I.I.S. experimentally reconstructed the director fields induced by colloids and compared them with theoretical results by modelling 3PEF-PM images. M.R., S.Ž. and I.I.S. analysed models of director fields and defects satisfying topological constraints. A.M., M.R. and I.I.S. wrote the manuscript. I.I.S. conceived and designed the project.

Additional information

Supplementary information is available in the online version of the paper. Reprints and permissions information is available online at www.nature.com/reprints. Correspondence and requests for materials should be addressed to I.I.S.

Competing financial interests

The authors declare no competing financial interests.

263